Received September 8, 2020, accepted October 25, 2020, date of publication November 20, 2020,
date of current version December 7, 2020.

Digital Object Identifier 10.1109/ACCESS.2020.3039524

Transient Atomization Modeling and Optimal Design of a Medical Air-Compressing Nebulizer

MINGHAO YU[1], RUI WANG[1], JIAFENG YAO[2], (Member, IEEE), KAI LIU[1], AND YUXUAN HAN[3]

[1]School of Mechanical and Precision Instrument Engineering, Xi'an University of Technology, Xi'an 710048, China
[2]College of Mechanical and Electrical Engineering, Nanjing University of Aeronautics and Astronautics, Nanjing 210016, China
[3]School of Automation, Xi'an University of Posts and Telecommunication, Xi'an 710121, China

Corresponding author: Yuxuan Han (CC_hanyuxuan@hotmail.com) and Jiafeng Yao (jiaf.yao@nuaa.edu.cn)

This work was supported in part by the National Natural Science Foundation of China under Grant 11705143, and in part by the Foundation for Research and Development of Applied Technology in Beilin District of Xi'an under Grant GX2047.

ABSTRACT This paper studies three-dimensional transient flow characteristics of a medical air-compressing nebulizer which is widely used to treat respiratory diseases in the medical field. The transient atomization process of air and water was numerically simulated and reproduced by solving Navier-Stokes equations, turbulent transport equations, the volume of fluid (VOF) model, and discrete phase model (DPM). The water volume fraction inside the nebulizer was simulated and demonstrated under different time. Besides, to better the working performance of the nebulizer, the effects of different working parameters such as different orifice diameters, length of the outflow pipe, and air velocity on the secondary atomization were also studied and discussed. It was found that the most suitable diameter of the orifice for this air-compressing nebulizer is 1.0 mm. Most suitable length of the outflow pipe and the air velocity for producing small air-water bubbles are 10 mm and 4 m/s, respectively.

INDEX TERMS Air-compressing nebulizer, atomization, droplet diameter, droplet break.

I. INTRODUCTION

The medical air-compressing nebulizer is one of important instruments to treat respiratory diseases in the medical field. The nebulizer can atomize the liquid medicine into tiny liquid droplets, and then the medicine enters the respiratory tract and lungs using breathing to achieve a painless, rapid, and effective treatment. Thus, it is widely used to treat respiratory diseases such as fever, cough, rhinitis, bronchitis, pneumonia, etc. In recent years, respiratory diseases have become increasingly serious all over the world. For example, atypical pneumonia had happened due to the SARS virus in 2002 [1]. Corona Virus Disease has happened due to coronavirus from 2019 to now [2]. Severe pneumonia conditions force us to find good methods to cure patients or to reduce the pain of patients. A medical nebulizer is one of the auxiliary instruments to treat respiratory diseases. Regarding the traditional treatments of respiratory diseases such as oral drugs and intravenous injections [3], [4], patients absorb medicine slowly and are likely to cause some side effects [5]. Therefore, using a medical nebulizer to supply atomized medicine to the respiratory tract and lungs is a more effective, fast, and safe way to treat the respiratory diseases. The medical nebulizer has attracted much attention in past decades. And also, many medical nebulizer or atomizer can be found in the market today.

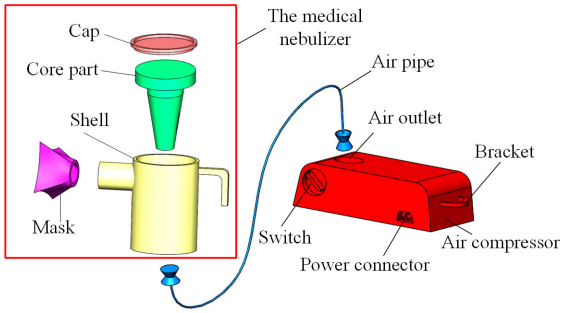

FIGURE 1. Medical nebulizer system.

Usually, the nebulizer has four types in the market: the gas-assisted atomizer, bubble atomizer, flat nozzle atomizer, and pressure swirl atomizer [6]. The composition of the medical air-compressing nebulizer system is shown in Fig. 1. It is composed of a power supply system and the medical nebulizer which includes a cap, core part, shell, and mask. When the nebulizer works, the air is compressed to reach a high-pressure state by the compressor firstly, and then the

The associate editor coordinating the review of this manuscript and approving it for publication was Zhixiong Peter Li.

compressed air is supplied to the bottom of the medical nebulizer. The high-pressure air can achieve a high speed, and can split the medical liquid to be tiny droplets.

In past decades, there are many numerical and experimental studies on the atomizer. For example, Eugenio used a conservative level-set to simulate the liquid atomization regimes [7]. Davide developed an improved multiscale Eulerian-Lagrangian method for simulating the atomization process [8]. Muhammad studied the viscous and frictional losses in pressure swirl atomizers [9]. Ji-Hun used a polymer micro atomizer for cone jet mode electrospray of water [10]. Deshpande builds instability predictions of liquid sheets injected into a gas medium to simulate the dynamics in the near-nozzle region [11]. Jheng-Jhih developed a piezoelectric atomizer [12]. Lelong use Fluent to optimize the design of a jet atomizer [13]. Sermsri modified a small volume jet nebulizer to fit Asthmatic Children [14]. About the medical air-compressing nebulizer, it uses the gas-assisted dual-fluid equipment to atomize the medical liquid. It includes two atomization processes: the first and the second atomizations. The first atomization is that the water column is separated into ribbon-shaped flakes water. The secondary atomization is that the ribbon-shaped flakes water becomes smaller water droplets [15]. Usually, the first atomization can be simulated by the VOF (volume of fluid) model [16]–[18], and the secondary atomization can be studied by DPM (discrete phase method) model [19], [20]. Recently, Yu *et al* numerically studied the flow-field properties of the gas-liquid dual-fluid atomizer which has high flow capacity and low energy consumption [21]. They found that an optimal orifice diameter exists to maximize the water flow velocity and the effeciency of the secondary atomization *etc*. As summary, although all these studies mentioned above are very encouraging and helpful for improving the working performance of the nebulizer or atomizer, there lacks a detailed study to demonstrate the complete transient atomization process clearly inside a medical nebulizer. Moreover, the atomized particle size of ordinary nebulizers currently on the market is generally in the 10-micron level, which is not conducive to the liquid entering the human lower respiratory tract and alveoli. The allowable droplet diameter of each part of the human respiratory tract is illustrated in Fig. 2.

Thus, in this study the three-dimensional time-dependent transient two-phase flow characteristics of the medical air-compressing nebulizer developed by us recently are simulated and analyzed by using the commercial software-FLUENT. The fluid domain of the nebulizer is constructed by the software SOLIDWORKS. The VOF multiphase flow model is employed to simulate the first atomization process, and the DPM model is employed to simulate the second atomization process. Usually, the atomization velocity, atomization efficiency, and liquid particle diameter were used to evaluate the working performance of a nebulizer [21]. So, in present study the diameter of atomization particles is used to evaluate the working performance of the nebulizer.

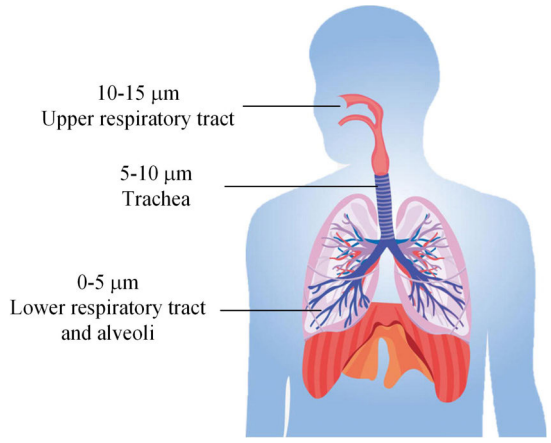

FIGURE 2. Allowable droplet diameter of each part of the human respiratory tract.

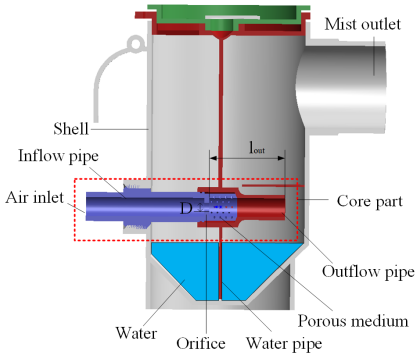

(a) Physical structure.

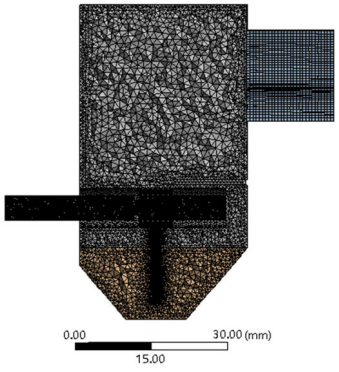

(b) Computational mesh.

FIGURE 3. Physical structure and the computational grid of the medical air-compressing nebulizer.

This paper is organized as follows: first, the influence of the grid number on present numerical simulation is discussed and verified. Second, the basic flow characteristics inside the air-compressing nebulizer are discussed and summarized. The transient atomization process and the mutual interaction between air and water are demonstrated by a time-variation video. Finally, to better the working performance of the nebulizer, the effects of the structural and working parameters such as the orifice diameter and the gas velocity are studied and discussed, respectively. The results of the present study could

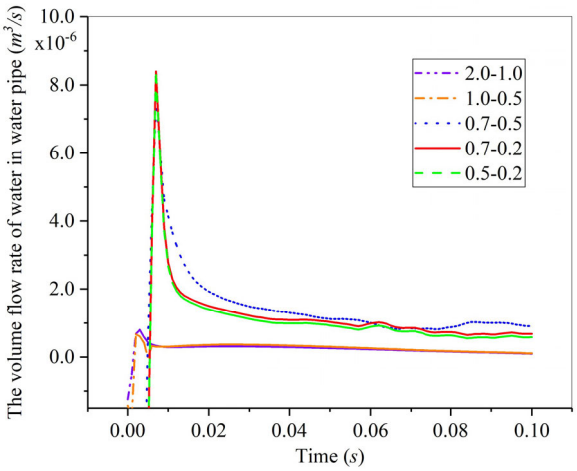

FIGURE 4. The volume flow rate of water in the water pipe under different grid sizes.

provide a more thorough comprehension of the atomization process for a medical nebulizer. Moreover, it also could provide theoretical guidance for the optimal design of a medical air-compressing nebulizer.

II. FORMULATION OF THE PROBLEM

A. COMPUTATIONAL DOMAIN AND VALIDATIONS OF GRID-INDEPENDENCE

The physical structure of the medical air-compressing nebulizer is shown as Fig. 3(a). The nebulizer includes two parts: the shell and the core part which is composed of the inflow pipe, the orifice, the water pipe, the porous medium, and the outflow pipe.

As the nebulizer starts to work, the high-speed air enters the inflow pipe from air inlet firstly, and then passes through the orifice, and generates a negative pressure at porous medium. Thereafter, the liquid at the bottom of the shell is absorbed into the water pipe automatically due to the negative pressure. The absorbed water column is primarily broken up to be ribbon-shaped flakes water by high-speed air at the porous medium section. Thereafter, the flakes water is broken further to be many water droplets in the outflow pipe. Finally, the water droplets will be taken out by air from the outlet of the air-compressing nebulizer.

Fig. 3(b) shows the computational domain and mesh of the nebulizer. To eliminate the effect of grid size on the numerical results, several test cases with different size grids of the nebulizer were performed before starting this study. Fig. 4 shows the distribution of the time-varying volume flow rate of water in the water pipe. The number "2.0-1.0" in Fig. 4 represents that the maximum volume of the shell mesh is 2.0 mm^3, and the maximum volume of the core part mesh is 1.0 mm^3. So does others in the legend of Fig. 4. It can be seen from Fig. 4 that the results hardly change as the maximum grid sizes of the shell and the core part are less than 0.7 and 0.2 mm^3 respectively. Therefore in this paper we adopt the mesh sizes "0.7-0.2" for all simulations. The total number of the computational grids for this nebulizer being 832046 is adopted for all simulations in this study.

TABLE 1. Grids number in figure 4.

	core part mesh(mm^3)	shell mesh(mm^3)	total computational grids
1	1	2	97234
2	0.5	1	307934
3	0.5	0.7	607357
4	0.2	0.7	832046
5	0.2	0.5	2098326

B. FLOW-FIELD EQUATIONS

This paper assumes that the flow state is turbulent and transient in the medical air-compressing nebulizer. For simplicity, pure water is used instead of medical mixing solutions. Air and water are thought to be incompressible, and regardless of heat exchange. The mass conservation and the momentum conservation equations are written as follows:

Mass conservation equation:

$$\frac{\partial u}{\partial x}+\frac{\partial v}{\partial y}+\frac{\partial w}{\partial z}=0. \tag{1}$$

u, v, w are velocity components in x, y, and z directions in the Cartesian system.

Momentum conservation equations:

$$\frac{\partial(\rho u)}{\partial t}+div(\rho uU)=-\frac{\partial p}{\partial x}+\frac{\partial \tau_{xx}}{\partial x}+\frac{\partial \tau_{yx}}{\partial y}+\frac{\partial \tau_{zx}}{\partial z}+F_x, \tag{2}$$

$$\frac{\partial(\rho v)}{\partial t}+div(\rho vU)=-\frac{\partial p}{\partial y}+\frac{\partial \tau_{xy}}{\partial x}+\frac{\partial \tau_{yy}}{\partial y}+\frac{\partial \tau_{zy}}{\partial z}+F_y, \tag{3}$$

$$\frac{\partial(\rho w)}{\partial t}+div(\rho wU)=-\frac{\partial p}{\partial z}+\frac{\partial \tau_{zx}}{\partial x}+\frac{\partial \tau_{yz}}{\partial y}+\frac{\partial \tau_{zz}}{\partial z}+F_z. \tag{4}$$

τ_{xy}, τ_{xx}, $\tau_{xz}\tau_{xy}$, τ_{xx}, τ_{xz} are viscous stress components respectively. F_x, F_y, $F_z\mathrm{F_x}$,$\mathrm{F_yF_z}$ are inertial forces in x, y, and z directions. In the present study, only gravity is considered as inertial force, so $F_x = F_y = 0\mathrm{F_x} = \mathrm{F_y}= 0$ and $F_z = -\rho g\mathrm{F_z}= -\rho\mathrm{g}$.

C. TURBULENT EQUATIONS

Several famous turbulence models such as Realized k-ε, Standard k-ε, Standard k-ω, RNG k-ε, BSL k-ω, and SST k-ω models are widely used to model the gas-liquid atomization process previously [22]. Generally, the SST k-ω model combines the advantages of k-ω model in the near-wall calculation and the advantages of k-ε model in the far-field calculation [23]. Besides, it is more applicable for simulating the gas-liquid two-phase flow with a backpressure gradient [21]. So, in this study, it employs the SST k-ω turbulent model to study the atomization process of the air-compressing nebulizer. The transport equations of SST k-ω model are as following [24]:

$$\frac{D(\rho k)}{Dt}=\widetilde{P}_k-\beta^*\rho k\omega+\nabla\cdot[(\mu+\sigma_k\mu_t)\nabla k], \tag{5}$$

$$\frac{D(\rho\omega)}{Dt}=\frac{\gamma}{\widehat{\nu}_t}-\beta\rho\omega^2+\nabla\cdot[(\mu+\sigma_k\mu_t)\nabla\omega]+2(1-F_1)\rho\sigma_{\omega2}\frac{1}{\omega}\nabla k\nabla\omega. \tag{6}$$

where the eddy viscosity is:

$$v_t = \frac{\mu_t}{\rho} = \frac{a_1 k}{\max\{a_1\omega, SF_2\}}, \tag{7}$$

$$\widehat{v_t} = \max\left\{v_t, 10^{-8}\right\}, \tag{8}$$

The production terms are:

$$P_k = \left[\mu_t\left(U_{i,j} + U_{j,i} - \frac{2}{3}U_{k,k}\delta_{ij}\right)\right]U_{i,j}, \tag{9}$$

$$\widetilde{P_k} = \min\left\{P_k, 10\beta^*\rho k\omega\right\}. \tag{10}$$

F_1 and F_2 are blending functions that depend on wall distance.

D. VOF MODEL FOR AIR-WATER TWO-PHASE FLOW

The VOF model based on multiphase flow theory is an effective numerical simulation method to track the interface between two or more immiscible fluids. In the calculation, all fluids share the turbulence model. And the interface is tracked by introducing the volume fraction of the i th phase, α_i, which satisfies $\sum_{i=1}^{n}\alpha_i = 1$ in each cell, where n is the number of phases. For air-water two-phase flow, α_w and α_a are respectively the volume fraction of water phase and air phase. For each control cell:

$$\alpha_a + \alpha_w = 1. \tag{11}$$

In each cell, if it contains only water, then $\alpha_w = 1$; if none, then $\alpha_w = 0$. For cells that contain the air-water interface, $0 < \alpha_w < 1$. When simulating the air-water interface, the volume fraction equation for water phase can be written as

$$\frac{\partial\alpha_w}{\partial t} + \vec{v}\cdot\nabla\alpha_w = 0. \tag{12}$$

The fluid properties in each cell are adjusted according to the volume fraction, for example, the fluid density in each cell is,

$$\rho = \alpha_w\rho_w + (1-\alpha_w)\rho_a. \tag{13}$$

Which is similar to the expression of the molecular viscosity μ.

E. DISCRETE PHASE MODEL (DPM)

A representative particle in each computational cell is solved in the Lagrangian frame and is extended to other particles. The force balance equation of motion for particles is as follows:

$$m_p\frac{d\vec{u}_p}{dt_p} = F_{drag} + m_p\frac{\vec{g}(\rho_p-\rho_c)}{\rho_p} + F_{lift} + F_{virtual} + F_{magnus} + F_b + F_{pressure}. \tag{14}$$

The interaction forces in the particle motion equation are briefly explained as follows. The drag force, which is valid for any ranges of Reynolds number, is as follows:

$$F_{drag} = \frac{m_p}{\tau}\frac{C_D Re_p}{24C_c}\left(u_c - u_p\right), \tag{15}$$

where

$$Re_p = \frac{\rho_c d_p\left|u_c - u_p\right|}{\mu_c}. \tag{16}$$

The lift force is given by:

$$F_{=lift} 20.3\mu_c d_p^2(u_c u_p)\sqrt{\frac{\dot{\gamma}\rho_c}{\mu_c}}sgn(\dot{\gamma}) \tag{17}$$

where $\dot{\gamma}$ is the shear rate which is mainly important at the vicinity of the walls. The pressure gradient and virtual mass forces are given as:

$$F_{pressure} = m_p\left(\frac{\rho_c}{\rho_p}\right)u_p\nabla u_c, \tag{18}$$

$$F_{virtual} = 0.5m_p\left(\frac{\rho_c}{\rho_p}\right)\frac{d}{dt}\left(u_c - u_p\right). \tag{19}$$

The general form of the Magnus lift force can be written as:

$$F_{magnus} = \frac{1}{2}A_p C_{ML}\rho_c\frac{\left|u_c - u_p\right|}{|\Omega|}\left[\left(u_c - u_p\right)\times\Omega\right], \tag{20}$$

$$C_{ML} = 0.45 + \left(\frac{Re_{\omega_p}}{Re_p} - 0.45\right) \times \exp\left(-0.05684Re_{\omega_p}^{0.4}Re_p^{0.3}\right). \tag{21}$$

where A_p and C_{ML} are the projected particle surface area and the rotational lift coefficient, respectively. This correlation is valid for $Re_p < 2000$. The default form of Brownian motion force is as follows:

$$F_b = \zeta_i\sqrt{\frac{6\pi d_p\mu_c K_B T}{t_p}}. \tag{22}$$

where ζ_i is the unit variance random number produced by a Gaussian white noise process. The following equation is chosen and implemented for Gaussian white noise function:

$$\zeta_1 = \sqrt{-2\ln U_1}\cos\left(2\pi U_2\right), \tag{23}$$

$$\zeta_2 = \sqrt{-2\ln U_1}\sin\left(2\pi U_2\right), \tag{24}$$

where U_i is uniform random numbers defined in the program. The final form of the code produces random values in each direction. For random values $U < 0.5$, ζ_1 is applied in the Brownian force, and else ζ_2 is adopted.

F. BOUNDARY AND WORKING CONDITIONS

The inlet is set as velocity boundary. The outlet is set as pressure boundary, and the pressure is set to be standard atmospheric pressure. The surface tension coefficient of gas-liquid two phases is set to be 0.073 N/m [25]. The gravity is 9.8 m/s^2. The porosity of the porous medium is set to be 0.1. At the bottom of the shell, water is static at the initial time. The physical properties of air and water are shown in Table 2. The working conditions of all computational cases are listed in Table 3.

III. RESULTS AND DISCUSSION

In this section, first, the basic characteristics of the transient atomization process inside the air-compressing nebulizer are discussed and analyzed under the typical working conditions of case 1 given in Table 3 above. The mutual interaction between air and water is demonstrated for case 1 under

TABLE 2. Physical properties of fluid masteries.

Fluid	density /(kg/m^3)	Viscosity /(pa·s)
water	998.2	1.003×10^{-3}
Air	1.29	1.7894×10^{-5}

TABLE 3. Working conditions of all computational cases.

Computational cases	1	2	3	4
Orifice diameter (D), mm	13.8	10	10	10
Length of outflow pipe (l_{out}), mm	20.5	6	10	15
Velocity of air (V), m/s	50	50	50	50

5	6	7	8	9	10	11	12	13
10	1	5	16	10	10	10	10	10
20	6	6	6	6	6	6	6	6
50	50	50	50	2	4	6	8	10

different time. Thereafter, the effects of different parameters such as different orifice diameters, gas velocity, and length of the outflow pipe on the bubble diameter are examined and discussed, respectively.

A. BASIC FLOW FEATURES OF THE ATOMIZATION PROCESS

Fig. 5 shows the atomization process of water and air at a different time with the volume fraction of water is in the range of 0-0.01 inside the air-compressing nebulizer. As can be seen from Fig. 5, the red part indicates water at the bottom of the nebulizer at the initial moment as shown in Fig. 5(a). First, the water surface in the water pipe will be pressed downward temporarily due to the increased pressure of the air at 1.4 ms as shown in Fig. 5(b). Second, the negative pressure is generated near the porous media, and then the water was absorbed and starts to go into the porous medium at 30 ms as shown in Fig. 5(c). Finally, the water is atomized gradually by the shear of air at 40 ms as shown in Fig. 5(d). It can be clearly seen that the atomized liquid fills in the entire nebulizer, and flows out gradually. The multimedia view of Fig. 5 is as the attached animation.

B. MODEL VALIDATION

To validate the accuracy of the numerical models used in this study, we performed a simulation for the core part of the nebulizer given in the experimental study [26] under the working conditions of the case 1. Fig. 6 shows the comparison of the simulated and the measured droplets diameters. It can be seen from Fig. 6 that the droplet diameters obtained in this simulation are generally consistent with the measured droplet diameters in the experimental study [26]. The maximum absolute error between the simulation and the experiment is

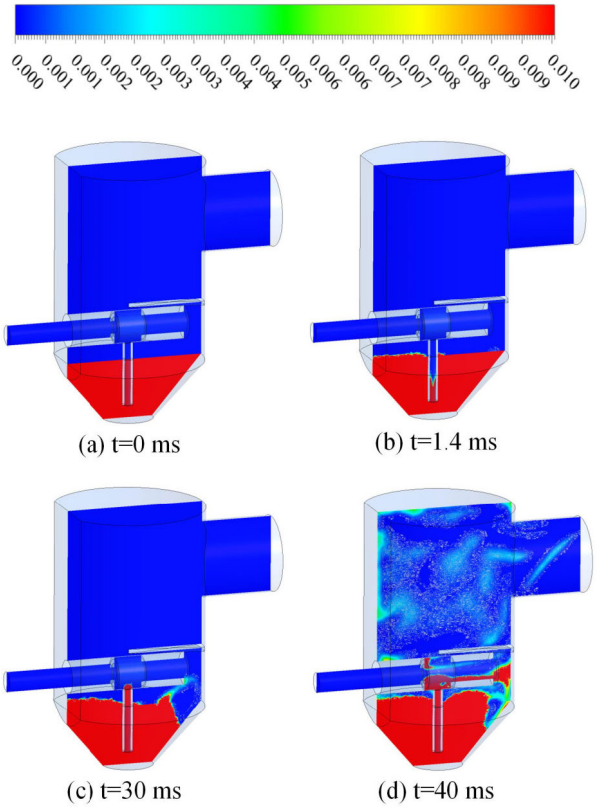

FIGURE 5. Atomization process of water and air in the nebulizer at a different time with the volume fraction of water is in the range of 0-0.01 (Multimedia view is as the attachment).

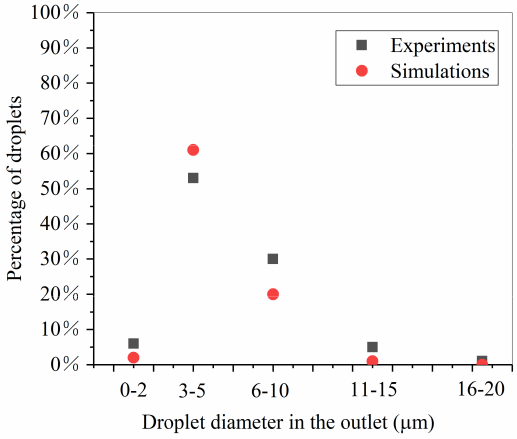

FIGURE 6. Atomized droplet diameter of experiments and simulations.

less than 10%. Such difference between the experiment and the simulation is probably caused by the uncertainty of the breakup model used in the simulation.

Because the DPM model involves many interaction forces, there are some uncertainties in the factors that affect these interaction forces, such as C_{ML}, Re_p, ζ_i, and these uncertain factors are likely to be the main reasons for errors in experiments and simulations. To minimize the simulation statistic error, we analyzed more than 200000 droplets diameters in the simulation in present study.

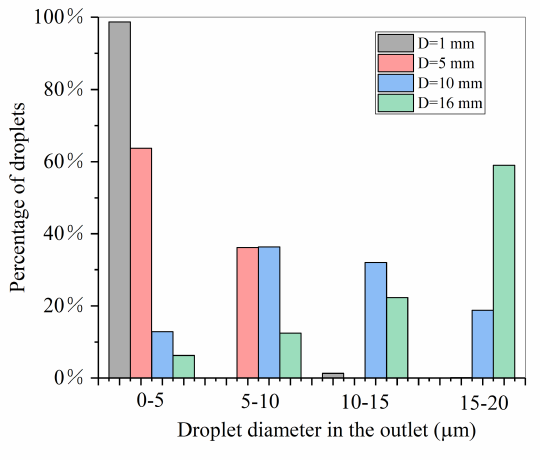

FIGURE 7. Atomized droplets diameter of the core part of the medical air-compressing nebulizer with different orifice diameter.

C. INFLUENCE OF THE ORIFICE DIAMETER

Fig. 7 shows the distributions of atomized droplet diameters at the outlet of the outflow pipe under different orifice diameters $D = 1.0$, 5.0, 10.0 and 16.0 for the computational case 2 and cases 6-8. Each calculation example counts about 200,000 droplets. As shown in the figure, when the orifice diameter is 1.0 mm, the atomized droplets with the diameter being 0 - 5 μm account for 98.71%. When the orifice diameter is 5 mm, the atomized droplets with the diameter being 0 - 5 μm account for 63.72%, and the droplets with the diameter being 5-10 μm account for 36.12%. When the orifice diameter is 10 mm, the atomized droplets with the diameter being 0 - 5 μm just account for 12.88%, and the droplets with the diameter being 5-10 μm account for 36.33%. Similarly, when the orifice diameter is 16 mm, the atomized droplets with the diameter being 0 - 5 μm just only account for 6.28%, and the droplets with the diameter being 15 - 20 μm are main, and account for 59.01%. Because the smaller the droplet diameter is, the easier it is for the liquid medicine to enter the lower respiratory tract and deep lungs. Therefore, the most suitable orifice diameter is 1.0 mm for treating respiratory diseases.

Fig. 8 shows the distribution of pressure in the outflow pipe for the computational case 2 and cases 6-8. As can be seen form Fig. 8, the negative pressure increases with the decrease of the orifice diameter. The pressure could reach -4.0×10^{10} pa when the orifice diameter is 1.0 mm. The greater the negative pressure, the better the water absorption. When the orifice diameter is 1.0 mm the diameter of the most atomized droplet is 0 - 5 μm. Therefore, the best orifice diameter is 1.0 mm for producing small droplets.

In addition, because the geometry of the core part will create a negative pressure at the porous medium, so when the droplets flow out the porous medium, they will flow slowly perpendicular to the axis of the outlet pipe first, and finally they are taken out fast from the outlet pipe by the high speed air. when the droplet moves in the direction perpendicular to the axis, the high-speed air has the greatest shearing effect on water, while when air and water droplets move in the

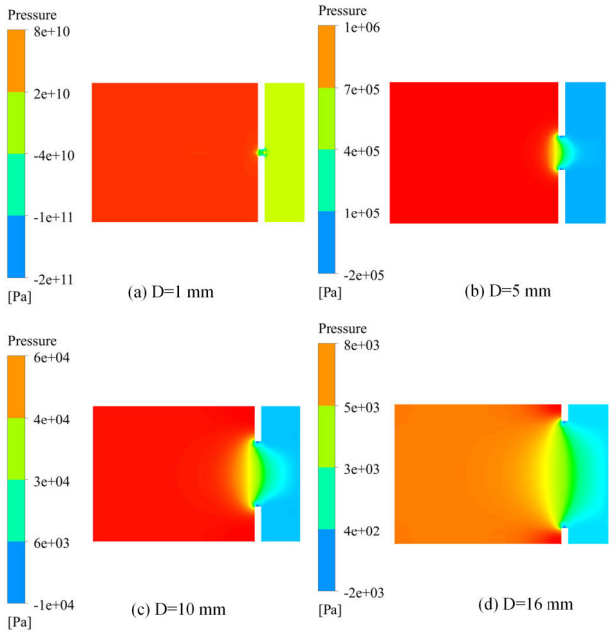

FIGURE 8. The pressure of the core part of the medical air-compressing nebulizer with different orifice diameter.

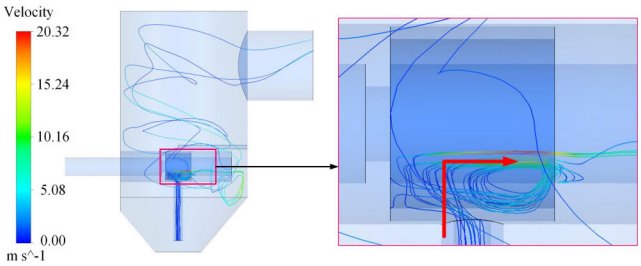

FIGURE 9. Distributions of streamlines for the water phase in the outflow pipe and in the whole nebulizer.

same direction, the shearing effect is minimal. In addition the vortex would make the shearing effect repeat. Threrfore, when the droplet moves in the direction perpendicular to the axis, it has a high probability to be sheared and broken by the vortex of air which can be seen in Fig. 9 in the outflow pipe. while when the droplet is carried by air, and flows along the axis of the outlet pipe, they move fast with 20 m/s, the shearing effect is minimal, therefore the probability of breaking is small. Therefore, the smaller diameter atomized droplet when the orifice is smaller.

D. INFLUENCE OF THE OUTFLOW PIPE LENGTH

Fig. 10 shows the distribution of atomized droplets diameter of the core part for the nebulizer under different outflow pipe length. for the computational cases 2-5. When the length of the outlet pipe is 6 mm, the atomized droplets with the diameters being 0 - 5 μm, 5 - 10 μm, 10 - 15 μm and 15 - 20 μm account for 12.88%, 36.33%, 32.02%, and 18.77%, respectively. When the length of the outlet pipe is 10 mm, the atomized droplets with the diameters being 0 - 5 μm, 5 - 10 μm, 10 - 15 μm and 15 - 20 μm account for 28.93%,

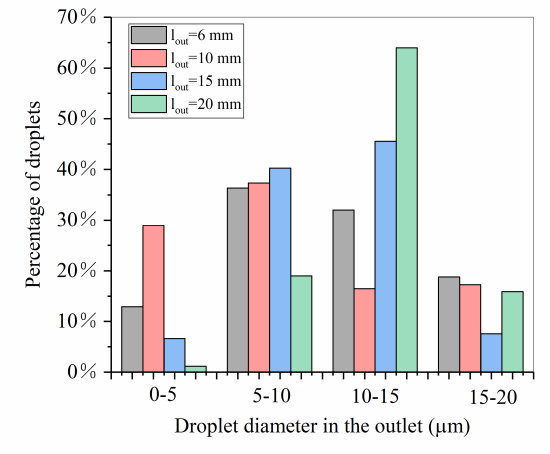

FIGURE 10. Atomized droplets diameter of the core part for the medical air-compressing nebulizer under different outflow pipe length.

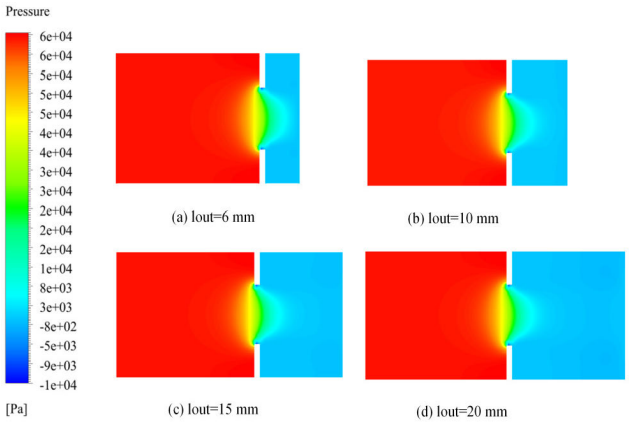

FIGURE 11. The pressure in the core part of the medical air-compressing nebulizer under different outflow pipe length.

37.31%, 16.49%, and 17.27%, respectively. When the length of the outlet pipe is 15 mm, the atomized droplets with the diameters being 0 - 5 μm, 5 - 10 μm, 10 - 15 μm and 15 - 20 μm account for 6.61%, 40.27%, 45.55%, and 7.57%, respectively. Similarly, when the length of the outlet pipe is 20 mm, the atomized droplets with the diameters being 0 - 5 μm, 5 - 10 μm, 10 - 15 μm and 15 - 20 μm account for 1.16%, 18.97%, 63.97%, and 15.89%, respectively. Because the smaller the droplet diameter, the better the effect of treating respiratory diseases, so according to the data given above it can conclude that the most suitable length of the outlet pipe is 10 mm for this nebulizer.

Fig. 11 shows the distribution of pressure in the core part of the nebulizer under different outflow pipe length for the computational cases 2-5. There is almost no change in pressure with the varation of the outlet pipe length. It indicates that the length of the outlet pipe has almost no effect on the pressure distribution. This lead to the same negative pressure and the same water absorption for the cases 2 - 5.

E. INFLUENCE OF AIR VELOCITY

Fig. 12 shows the distributions of atomized droplets diameter at the core part of the nebulizer under different air velocity for

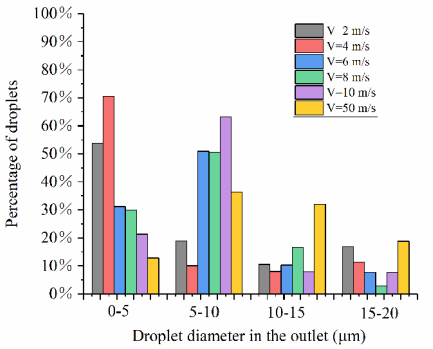

FIGURE 12. Atomized droplets diameter at the core part of the medical air-compressing nebulizer under different air velocity.

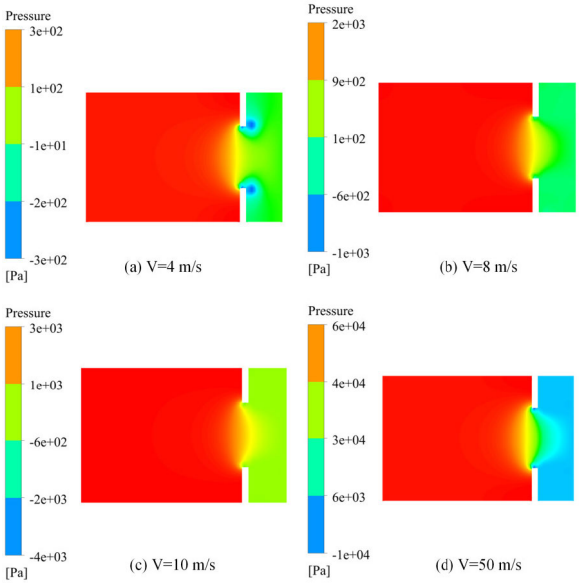

FIGURE 13. The pressure in the core part of the medical air-compressing nebulizer under different air velocity.

the computational case 2 and cases 9-13. When the velocity is 2 m/s and 4 m/s, the atomized droplets with the diameter being 0 - 5 μm could account for 53.72% and 70.60%, respectively. When the velocity is greater than 4 m/s, the droplets with the diameter being 0 - 5 μm decrease with the increment of the air velocity. In addition, as the air velocity is 4 m/s, the droplet diameter of 5-20 μm keeps at a low level. Because the smaller the droplet diameter is, the better the effect of treating respiratory diseases is. So, the optimal velocity of air is 4 m/s for this nebulizer.

Fig. 13 shows the distribution of pressure in the core part of the nebulizer under different air velocity for the computational case 2 and cases 9-13. As can be seen from the figure, the negative pressure increases with the increment of the air velocity. Although greater negative pressure leads to better absorption effects of water, the atomized droplet diameter become larger when the air velocity is bigger than 6 m/s. For the above situation, when the air velocity is small *e.g.*, 2 m/s, its momentum and kinetic energy are all small, so then air cannot play a good role in shearing droplets. In contrast,

when the air velocity is very high *e.g.*, 50 m/s, the droplets will be taken out fast before being sheared from the outlet pipe. It also leads to low breakup efficiency of water. So, there exists an optimal air velocity to get smallest droplets. As shown in Fig. 13, we can see that the optimal air velocity is 4 m/s for producing most smallest droplets.

IV. CONCLUSION

Three-dimensional transient atomization process inside a medical air-compressing nebulizer was numerically modeled by solving Navier-Stokes equations coupled with the SST k-ω turbulent transport equations. The time-variation trends of water volume fraction inside the nebulizer are simulated and demonstrated clearly. The negative pressure is generated in the porous medium section; it results in the static water automatically flowing into the water pipe. Besides, it concluded that the diameter of the atomized particle diameter reduces with the decrease of orifice diameter through the present study. The most suitable diameter of the orifice for the air-compressing nebulizer presented in this study is 1.0 mm. There are suitable outflow pipe length and velocity for producing small bubbles, they are 10 mm and 4 m/s respectively. The droplets are mainly sheared and broken from the porous medium to the orifice.

REFERENCES

[1] R. He, F. Dobie, M. Ballantine, A. Leeson, Y. Li, N. Bastien, T. Cutts, A. Andonov, J. Cao, T. F. Booth, F. A. Plummer, S. Tyler, L. Baker, and X. Li, "Analysis of multimerization of the SARS coronavirus nucleocapsid protein," *Biochem. Biophys. Res. Commun.*, vol. 316, no. 2, pp. 476–483, Apr. 2004.

[2] M. A. Shereen, S. Khan, A. Kazmi, N. Bashir, and R. Siddique, "COVID-19 infection: Origin, transmission, and characteristics of human coronaviruses," *J. Adv. Res.*, vol. 24, pp. 91–98, Jul. 2020.

[3] C.-C. Lim, I.-C. Peng, and Y.-H. Huang, "Safety of intrastromal injection of polyhexamethylene biguanide and propamidine isethionate in a rabbit model," *J. Adv. Res.*, vol. 22, pp. 1–6, Mar. 2020.

[4] S. Hossen, M. K. Hossain, M. K. Basher, M. N. H. Mia, M. T. Rahman, and M. J. Uddin, "Smart nanocarrier-based drug delivery systems for cancer therapy and toxicity studies: A review," *J. Adv. Res.*, vol. 15, pp. 1–18, Jan. 2019.

[5] R. A. Tawfiq, N. N. Nassar, W. I. El-Eraky, and E. S. El-Denshary, "Enhanced efficacy and reduced side effects of diazepam by kava combination," *J. Adv. Res.*, vol. 5, no. 5, pp. 587–594, Sep. 2014.

[6] Y. Yuan, "Numerical simulation of gas-liquid two-phase flow in effervescent atomizer," *J. shaanxi Univ. Sci. Technol.*, vol. 33, no. 05, pp. 135–140, Oct. 2015.

[7] E. Schillaci, O. Antepara, N. Balcázar, J. R. Serrano, and A. Oliva, "A numerical study of liquid atomization regimes by means of conservative level-set simulations," *Comput. Fluids*, vol. 179, pp. 137–149, Jan. 2019.

[8] J. L. Estivalèzes and D. B. Zuzio Dipierro, "An improved multiscale Eulerian-Lagrangian method for simulation of atomization process," *Comput. Fluids.*, vol. 176, no, pp. 65–77, Nov. 2016.

[9] M. Rashad, H. Yong, and C. Bin, "Study of viscous and frictional losses in pressure swirl atomizers," in *Proc. 13th Int. Bhurban Conf. Appl. Sci. Technol. (IBCAST)*, Jan. 2016, pp. 490–496.

[10] J.-H. Jeong, H. Choi, J. Choi, and S. S. Lee, "Polymer micro atomizer for cone jet mode electrospray of water," in *Proc. IEEE 33rd Int. Conf. Micro Electro Mech. Syst. (MEMS)*, Jan. 2020, pp. 1114–1117.

[11] S. S. Deshpande, S. R. Gurjar, and M. F. Trujillo, "A computational study of an atomizing liquid sheet," *Phys. Fluids*, vol. 27, no. 8, Aug. 2015, Art. no. 082108.

[12] J.-J. Huang and C.-T. Chen, "Microelectroforming of a nickel nozzle plate featured with anti-stiction for a piezoelectric atomizer," in *Proc. 8th Annu. IEEE Int. Conf. Nano/Micro Eng. Mol. Syst.*, Apr. 2013, pp. 490–493.

[13] N. Lelong, L. Vecellio, Y. Sommer de Gélicourt, C. Tanguy, P. Diot, and A. Junqua-Moullet, "Comparison of numerical simulations to experiments for atomization in a jet nebulizer," *PLoS ONE*, vol. 8, no. 11, Nov. 2013, Art. no. e78659.

[14] S. J. Santati Thongsri and P. Sarntima, "Modified small-volume jet nebulizer based on CFD simulation and its clinical outcomes in small asthmatic children," *J. Healthcare Eng.* vol. 2019, Jun. 2019, Art. no. 2524583.

[15] M. Xia, "Computational fluid dynamic investigation of the primary and secondary atomization of the free-fall atomizer in electrode induction melting gas atomization process," *Acta. Physica. Sinica.*, vol. 67, no. 17, pp. 1–12, 2018.

[16] U. Fritsching, *Spray Simulation*. Cambridge, U.K.: Cambridge Univ. Press, Apr. 2004, p. 286.

[17] N. Zeoli, H. Tabbara, and S. Gu, "CFD modeling of primary breakup during metal powder atomization," *Chem. Eng. Sci.*, vol. 66, no. 24, pp. 6498–6504, Dec. 2011.

[18] Y. Liu, "Flow field of double layer atomizer," *Aeronaut. J.*, vol. 35, no. 5, pp. 63–69, 2015.

[19] D. A. Firmansyah, S.-G. Kim, K.-S. Lee, R. Zahaf, Y. H. Kim, and D. Lee, "Microstructure-controlled Aerosol–Gel synthesis of ZnO quantum dots dispersed in SiO2 nanospheres," *Langmuir*, vol. 28, no. 5, pp. 2890–2896, Jan. 2012.

[20] J. S. Thompson, O. Hassan, S. A. Rolland, and J. Sienz, "The identification of an accurate simulation approach to predict the effect of operational parameters on the particle size distribution (PSD) of powders produced by an industrial close-coupled gas atomiser," *Powder Technol.*, vol. 291, pp. 75–85, Apr. 2016.

[21] Y. Minghao, W. Rui, L. Kai, and Y. Jiafeng, "Numerical simulation of three-dimensional transient flow characteristics for a dual-fluid atomizer," *Eng. Appl. Comput. Fluid Mech.*, vol. 13, no. 1, pp. 1144–1152, Oct. 2019.

[22] C. Tian and Y. Lu, "Turbulence models of separated flow in shock wave thrust vector nozzle," *Eng. Appl. Comput. Fluid Mech.*, vol. 7, no. 2, pp. 182–192, Jan. 2013.

[23] F. R. Menter, "Zonal two equation k-w turbulence models for aerodynamic flows," Amer. Inst. Aeronaut. Astronaut., Long Beach, CA, USA, Tech. Rep. AIAA-93-2906, 1993.

[24] U. C. Goldberg and P. Batten, "A wall-distance-free version of the SST turbulence model," *Eng. Appl. Comput. Fluid Mech.*, vol. 9, no. 1, pp. 33–40, Mar. 2015.

[25] J. D. Wright, V. E. Bean, and J. Aguilera, "NIST calibration services for hydrometers," Nat. Inst. Standards Technol., Gaithersburg, MD, USA, Tech. Rep. SP-250-78, Jun. 2020, pp. 11–12.

[26] J. Yao, S. Furusawa, A. Kawahara, and M. Sadatomi, "Influence of some geometrical parameters on the characteristics of prefilming twin-fluid atomization," *Trans. Can. Soc. Mech. Eng.*, vol. 38, no. 3, pp. 391–404, Sep. 2014.

MINGHAO YU received the Ph.D. degree from Kyushu University, Fukuoka, Japan, in 2015. He is currently an Associate Professor with the Xi'an University of Technology, Xi'an, China. His current research interests include optimal design and flow-field simulation of high-frequency inductive plasma wind tunnels and air-compression dual-fluid atomizers.

RUI WANG received the B.S. degree in mechanical engineering from Xi'an Shiyou University, Xi'an, China, in 2018. He is currently pursuing the M.S. degree in mechanical engineering with the School of Mechanical and Precision Instrument Engineering, Xi'an University of Technology. His research interests include the structural optimizations of atomizers and diesel injectors.

JIAFENG YAO (Member, IEEE) received the Ph.D. degree from Kumamoto University, Kumamoto, Japan, in 2014. He is currently an Associate Professor with the Nanjing University of Aeronautics and Astronautics, Nanjing, China. His current research interests include multiphase flow measurement, biomedical measurement, and electrical impedance tomography.

KAI LIU was born in Xi'an, Shaanxi, China, in 1957. He received the Ph.D. degree from the Graduate School, Kinki University, Higashiosaka, Japan, in 2003. He is currently a Professor with the School of Mechanical and Precision Engineering, Xi'an University of Technology, works at teaching post-graduation students and scientific research. His research interests include mechanical system dynamics and measurement techniques of the mechanical systems and mechanical transmission.

YUXUAN HAN was born in Xi'an, Shaanxi, China, in 1982. She received the B.S. degree in electrical engineering from the Xi'an University of Technology, China, in 2004, and the Ph.D. degree in precision machinery engineering from Nihon University, Japan, in 2019.

Since 2019, she has been a Lecturer with the Electrical Engineering and Automation Department, School of Automation, Xi'an University of Posts and Telecommunications. Her research interests include microfluidic systems, MEMS, micro/nano-machining, and plasma etching.